



HAL
open science

Coherence resonance in random Erdős-Rényi neural networks: mean-field theory

Axel Hutt, T Wahl, N Voges, Jo Hausmann, J Lefebvre

► **To cite this version:**

Axel Hutt, T Wahl, N Voges, Jo Hausmann, J Lefebvre. Coherence resonance in random Erdős-Rényi neural networks: mean-field theory. 2021. hal-03244053v1

HAL Id: hal-03244053

<https://inria.hal.science/hal-03244053v1>

Preprint submitted on 1 Jun 2021 (v1), last revised 14 Jun 2021 (v2)

HAL is a multi-disciplinary open access archive for the deposit and dissemination of scientific research documents, whether they are published or not. The documents may come from teaching and research institutions in France or abroad, or from public or private research centers.

L'archive ouverte pluridisciplinaire **HAL**, est destinée au dépôt et à la diffusion de documents scientifiques de niveau recherche, publiés ou non, émanant des établissements d'enseignement et de recherche français ou étrangers, des laboratoires publics ou privés.

Coherence resonance in random Erdős-Rényi neural networks : mean-field theory

A. Hutt^{1,*}, T. Wahl¹, N. Voges², Jo Haussmann³, J. Lefebvre⁴

¹Team MIMESIS, INRIA Nancy Grand Est, Strasbourg, France

²ILCB & INT UMR 7289, Aix Marseille Université, Marseille, France

³R&D department, Hyland Switzerland Sarl, Geneva, Switzerland

⁴Krembil Research Institute, University Health Network, Toronto, Canada

Correspondence*:

A. Hutt

axel.hutt@inria.fr

2 ABSTRACT

3 Additive noise is known to tune the stability of nonlinear systems. Using a network of two
4 randomly connected interacting excitatory and inhibitory neural populations driven by additive
5 noise, we derive a closed mean-field representation that captures the global network dynamics.
6 Building on the spectral properties of Erdős-Rényi networks, mean-field dynamics are obtained
7 via a projection of the network dynamics onto the random network's principal eigenmode. We
8 consider Gaussian zero-mean and Poisson noise stimuli to excitatory neurons and show that
9 these noise types induce coherence resonance. Specifically, the stochastic stimulation induces
10 coherent stochastic oscillations at intermediate noise intensity. We further show that this is valid
11 for both global stimulation and partial stimulation, i.e. whenever a subset of excitatory neurons
12 is stimulated only. The mean-field dynamics exposes the coherence resonance dynamics by a
13 transition from a stable non-oscillatory equilibrium to an oscillatory equilibrium via a saddle-node
14 bifurcation. We evaluate the transition between non-coherent and coherent state by various power
15 spectra, spike-field coherence and information-theoretic measures.

16 **Keywords:** coherence resonance, phase transition, stochastic process, excitable system, mean-field, random networks

1 INTRODUCTION

17 Synchronisation is a well characterized phenomenon in natural systems [1]. A confluence of experimental
18 studies indicate that synchronization may be a hallmark pattern of self-organisation [2, 3, 4]. While
19 various mechanisms are possible, synchronization may emerge notably through an enhancement of internal
20 interactions or via changes in external stimuli statistics. A specific type of synchronisation can occur due to
21 random external perturbations, leading to a noise-induced coherent activity. Such a phenomenon is called
22 coherence resonance (CR) and has been found experimentally in solid states [5], nanotubes [6] and in neural
23 systems [7]. Theoretical descriptions of CR have been developed for single excitable elements [8, 9, 8],
24 for excitable populations [10] and for clustered networks [11].

25 In general, stimulus-induced synchronisation is well-known in neural systems [2]. Synchronisation has
26 been observed intracranially in the presence of noise between single neurons in specific brain areas [12, 13]

27 and between brain areas [14, 15, 16]. The source of these random perturbations is still under debate. In
 28 this context, it is interesting to mention that [17] have found that the ascending reticular arousal system
 29 (ARAS) affects synchronisation in the visual cortex. The ARAS provides dynamic inputs to many brain
 30 areas areas [18, 19, 20]. It has thus been hypothesized that synchronisation in the visual system represents a
 31 CR effect triggered by ARAS-mediated drive. This hypothesis has been supported recently by [21] showing
 32 in numerical simulations that an intermediate intensity of noise maximises the interaction in a neural
 33 network of Hodgkin-Huxley neurons. Furthermore, recent theoretical work [20] has provided key insights
 34 on how human occipital electrocorticographic γ -activity observed with open eyes [20] is closely linked to
 35 CR. Coherence resonance has further been associated with states of elevated information processing and
 36 transfer [21], which are difficult to assess in the absence of mean-field descriptions.

37 To better understand the mechanisms underlying CR and its impact on information processing, we
 38 consider a simple two-population Erdős-Rényi network of interconnected McCulloch-Pitts neurons. Our
 39 goal is to use this model to provide some insight into the emergence of stimulus-induced synchronisation
 40 in neural systems and its influence on the neural network's information content. The neural network under
 41 study has random connections, a simplification inspired from the lack structure neural circuits possess
 42 at microscopic scales. Previous studies [22] have shown that such systems are capable of noise-induced
 43 CR. Building on these results, we here provide a rigorous derivation of a mean-field equation based on an
 44 appropriate eigenmode decomposition to highlight the role of the network's connectivity - Erdős-Rényi
 45 more specifically - eigenspectrum in supporting accurate mean-field representations. We extend previous
 46 results by further considering both global (all neurons are stimulated) and partial (some neurons are
 47 stimulated) stochastic stimulation and its impact on CR similar to some previous studies [23, 24, 25]. This
 48 partial stimulation is both more general and realistic than global stimulation as considered in most previous
 49 studies [22, 10, 26]. We apply our results to both zero-mean Gaussian and Poisson stochastic stimuli, and
 50 derive the resulting mean-field description. It is demonstrated rigorously that partial stochastic stimulation
 51 shifts the system's dynamic topology and promotes CR, compared to global stimulation . We confirm and
 52 explore the presence of CR using various statistical measures.

2 MATERIAL AND METHODS

53 We first introduce the network model under study, motivate the mean-field description, mentions the
 54 nonlinear analysis employed and provides details on the statistical evaluation.

2.1 The network model

56 Generically, biological neuronal networks are composed of randomly connected excitatory and inhibitory
 57 neurons, which interact through synapses with opposite influence on post-synaptic cells. We assume neural
 58 populations of excitatory \mathcal{E} and inhibitory \mathcal{I} neurons with N neurons in each population. Excitatory neurons
 59 in \mathcal{E} excite each other through the connectivity matrix \mathbf{F} , and excite inhibitory neurons in \mathcal{I} through the
 60 connectivity matrix \mathbf{M} . Similarly, neurons in \mathcal{I} inhibit each other by \mathbf{F} and inhibit excitatory neurons
 61 through the connectivity matrix \mathbf{M} . Hence, \mathbf{F} and \mathbf{M} represent the intra-population and inter-population
 62 synaptic connections, respectively. Mathematically, such neural population interactions are described
 63 by a $2N$ -dimensional non-linear dynamical system governing the evolution of the state variable vectors

64 $\mathbf{V}, \mathbf{W} \in \mathbb{R}^N$,

$$\begin{aligned} \tau_e \frac{d\mathbf{V}}{dt} &= -\mathbf{V} + \mathbf{F}\mathbf{S}_1[\mathbf{V}] - \mathbf{M}\mathbf{S}_2[\mathbf{W}] + eI^e + \boldsymbol{\xi}^e(t) \\ \tau_i \frac{d\mathbf{W}}{dt} &= -\mathbf{W} + \mathbf{M}\mathbf{S}_1[\mathbf{V}] - \mathbf{F}\mathbf{S}_2[\mathbf{W}] + eI^i + \boldsymbol{\xi}^i(t). \end{aligned} \quad (1)$$

65 This formulation is reminiscent of many rate-based models discussed previously [27], where it is as-
 66 sumed that neuronal activity is asynchronous and synaptic response functions are of first order. The state
 67 variables \mathbf{V} and \mathbf{W} represent excitatory and inhibitory dendritic currents, respectively. The terms $\boldsymbol{\xi}^{e,i}$
 68 represent respective stochastic inputs from various sources, such as ion channel fluctuations, stochas-
 69 tic input from other brain areas or external stimuli not directly accounted for in the model [28].
 70 More specifically, we assume noise $\boldsymbol{\xi}^{e,i} \in \mathbb{R}^N$, constant input $I^{e,i}$ with $e = (1, \dots, 1)^t$. The con-
 71 nectivity matrices are defined by $\mathbf{F}, \mathbf{M} \in \mathbb{R}^{N \times N}$ while the nonlinear transfer function is given by
 72 $\mathbf{S}_{1,2}[\mathbf{u}] \in \mathbb{R}^N$ with $(\mathbf{S}_1[\mathbf{u}])_i = H_0 S(u_i)$, $(\mathbf{S}_2[\mathbf{u}])_i = S(u_i)$, $H_0 > 0$ and the scalar transfer function
 73 $S(u) > 0 \forall u \in \mathbb{R}$. Specifically, we will consider the transfer function $S(u) = \Theta(u)$ with the Heaviside
 74 function $\Theta(u) = 0 \forall u < 0$, $\Theta(u) = 1 \forall u \geq 0$. In addition, the synaptic time scales are $\tau_{e,i}$.
 75

76 The present work considers directed Erdős-Rényi networks (ERN) with connection probability density
 77 $c = 0.95$, i.e. both neuron populations exhibit intra-population and inter-population non-sparse random
 78 connections. Let us assume $\mathbf{F} = \mathbf{A}F_0$, $\mathbf{M} = \mathbf{A}M_0$ and \mathbf{A} is the non-symmetric adjacency matrix of the
 79 ERN for which $(\mathbf{A})_{ij} = 0$ with probability $1 - c$ and $(\mathbf{A})_{ij} = 1/cN$ with probability c .
 80 At first, let $\mathbf{A} = \mathbf{S} + \mathbf{U}$ with the symmetric matrix $\mathbf{S} = (\mathbf{A} + \mathbf{A}^t)/2$, the antisymmetric matrix
 81 $\mathbf{U} = (\mathbf{A} - \mathbf{A}^t)/2$ and the eigenvalues λ_A and λ_S of the matrix \mathbf{A} and \mathbf{S} , respectively. Then $\mathcal{R}e(\lambda_A) = \lambda_S$,
 82 i.e. the real part of the eigenvalue spectrum in the directed (i.e. non-symmetric) and non-directed (i.e.
 83 symmetric) random matrix \mathbf{A} and \mathbf{S} is identical. Moreover, for non-directed ERNs with symmetric
 84 adjacency matrix and $N \rightarrow \infty$ its edge spectrum contains the maximum eigenvalue $\lambda_1 = 1$ with eigenvector
 85 $\mathbf{v}_1 = (1, 1, \dots, 1)^t$ [29, 30, 31, 32] and the bulk spectrum has the maximum eigenvalue

$$\begin{aligned} \lambda_2 &= \frac{2\sigma\sqrt{N}}{cN} \\ &= \frac{2\sqrt{1-c}}{\sqrt{cN}} \end{aligned} \quad (2)$$

86 with the corresponding Bernoulli distribution variance $\sigma^2 = c(1 - c)$. It is obvious that $\lambda_2 \ll \lambda_1$ and
 87 $\lambda_2 \approx 0$ for large mean degree cN . Since $\mathcal{R}e(\lambda_A) = \lambda_S$, the finite-size non-symmetric connectivity matrix
 88 \mathbf{F} (\mathbf{M}) has a maximum eigenvalue $\lambda_1 \approx F_0$ and $\lambda_{i>1} \approx 0$ ($\lambda_1 \approx M_0$, $\lambda_{i>1} \approx 0$). If c decreases, then λ_2
 89 increases, i.e. the spectral gap decreases, and this approximation does not hold anymore. The Appendix
 90 illustrates the limits of this approximation in numerical simulations.

91 Figure 1(A) shows the single maximum eigenvalue λ_1 of \mathbf{A} representing the edge spectrum and the other
 92 very small eigenvalues of the bulk spectrum. Hence, the matrix \mathbf{F} has maximum eigenvalue F_0 and the other
 93 eigenvalues vanish. The same holds for matrix $\mathbf{M} = M_0\mathbf{A}$ with a maximum eigenvalue M_0 . Figure 1(B)
 94 shows the real and imaginary part of the eigenvectors. The eigenvectors of the bulk spectrum ($i > 1$)
 95 have uniformly distributed elements in good accordance with theory of symmetric ER networks [33]. The
 96 eigenvector of the edge spectrum is $\Phi_1 = (1, \dots, 1)^t$, see Figure 1(C).

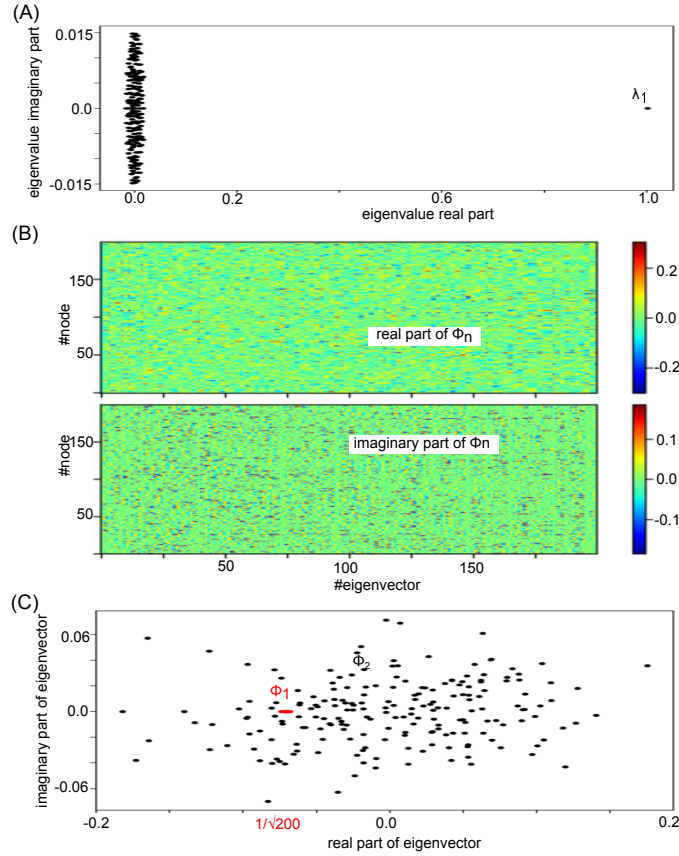


Figure 1. Eigenvalue spectrum of an Erdős-Rényi adjacency matrix A under study and its eigenbasis. (A) The plot shows the eigenvalues in the complex plane demonstrating a clear spectral gap between the first eigenvalue λ_1 and the other eigenvalues $\lambda_{n>1}$. (B) The panels show the real (top) and imaginary (bottom) part of all unit-normalized eigenvectors for illustration. They appear to be random reflecting the random network topology. (C) The normalized eigenvector $\Phi_1 \approx (1, \dots, 1)/\sqrt{N}$ with maximum eigenvalue $\lambda_1 \approx 1$ plotted in complex plane together with the eigenvector Φ_2 of the second largest eigenvalue $\lambda_2 = 0.015 + i0.0006$. Each dot corresponds to a complex-numbered vector entry in the complex plane. This result confirms the choice $\Phi_1 \approx (1, \dots, 1)$ in Eqs. (9).

97 Moreover, we assume that each noise process at inhibitory neurons $(\eta^i)_n = \eta_n^i$ at network node n is
 98 Gaussian distributed with zero mean, noise intensity D_2 and uncorrelated in time

$$\langle \xi_n^i(t) \xi_m^i(\tau) \rangle = 2D_2 \delta_{nm} \delta(t - \tau).$$

99 Conversely each noise process at excitatory neurons ξ_n^e belongs to a certain class $\mathcal{G}_m, m = 1, \dots, M$ of M
 100 classes [22]. Noise processes in a specific class \mathcal{G}_m , i.e. $n \in \mathcal{G}_m$, share their mean $\bar{\xi}_m^e$ and variances D_1^m ,
 101 i.e.

$$\langle \xi_k^e(t) \xi_l^e(\tau) \rangle = 2D_1^m \delta_{kl} \delta(t - \tau) \quad , \quad k, l \in \mathcal{G}_m.$$

102 In the following, we assume two classes $M = 2$ with $\bar{\xi}_1^e \neq 0$, $D_1^1 = D_1$ and $\bar{\xi}_2^e = 0$, $D_1^2 = 0$, i.e. only
 103 a subset of nodes $n \in \mathcal{G}_1$ are stimulated. Hence we consider a partial stimulation at number of nodes
 104 $N_1 = |\mathcal{G}_1|$.

105 In biological neural systems, the input to a neural population is well-described by incoming spike trains
 106 that induce dendritic currents at synaptic receptors. According to renewal theory, neurons emit spike trains
 107 whose interspike interval obeys a Poisson distribution [34]. Then incoming spike trains at mean spike
 108 rate r induce random responses at excitatory synapses with time constant τ_{in} . This random process $I_{in}(t)$
 109 has the ensemble mean $E[I_{in}] = w_{in}r\tau_{in}$ and ensemble variance $\text{Var}[I_{in}] = w_{in}^2r\tau_{in}/2$ [35] assuming the
 110 synaptic coupling weight w_{in} . Since a Poisson distribution converges to a Gaussian distribution for large
 111 enough mean, we implement this input current as a Gaussian random process with mean $E[I_{in}]$ and variance
 112 $\text{Var}[I_{in}]$ while ensuring the validity of this approximation by a large enough input firing rate λ_{in} . It is
 113 important to point out that for Poisson noise, in contrast to the zero-mean Gaussian noise, both mean and
 114 variance are proportional to the input firing rate.
 115

116 2.2 Conventional Mean-Field Analysis

117 To compare mesoscopic neural population dynamics to macroscopic experimental findings, it is
 118 commonplace to describe the network activity by the mean population response, i.e. the mean-field dynam-
 119 ics [36, 37, 38]. A naive mean-field approach was performed in early neuroscience studies [39, 40, 41], in
 120 which one blindly computes the mean network activity to obtain

$$\begin{aligned}\tau_e \frac{dE[V]}{dt} &= -E[V] + \mathbf{fS}_1[\mathbf{V}] - \mathbf{mS}_2[\mathbf{W}] + eI^e \\ \tau_i \frac{dE[W]}{dt} &= -E[W] + \mathbf{mS}_1[\mathbf{V}] - \mathbf{fS}_2[\mathbf{W}] + eI^i\end{aligned}\quad (3)$$

121 with the network average $E[x] = \sum_k x_k/N$ and $(\mathbf{f})_k = \sum_l \mathbf{F}_{lk}/N$, $(\mathbf{m})_k = \sum_l \mathbf{M}_{lk}/N$ assuming
 122 zero-mean external noise with $\sum_k (\boldsymbol{\xi}^{e,i})_k = 0$. In addition, one may assume identical network interactions
 123 with $(\mathbf{f})_k = f_0/N = \text{const}$, $(\mathbf{m})_k = m_0/N = \text{const}$ and the simplifying but questionable linear assumption

$$E[S_{1,2}(x)] = S_{1,2}(E[x]) . \quad (4)$$

124 Combined, these assumptions lead to mean-field equations

$$\begin{aligned}\tau_e \frac{dE[V]}{dt} &= -E[V] + f_0 S_1[E[V]] - m_0 S_2[E[W]] \\ &\quad + eI^e \\ \tau_i \frac{dE[W]}{dt} &= -E[W] + m_0 S_1[E[V]] - f_0 S_2[E[W]] \\ &\quad + eI^i\end{aligned}\quad (5)$$

125 In this approximate description, additive noise does not affect the system dynamics.
 126 The assumption (4) is very strong and typically not valid. In a more reasonable ansatz

$$\begin{aligned}
 & E[S_{1,2}(x)] \\
 &= E\left[S_{1,2}(x_0) + \sum_{n=1}^{\infty} \frac{1}{n!} S_{1,2}^{(n)}(x-x_0)^n\right] \\
 &= S_{1,2}(x_0) + \sum_{n=1}^{\infty} \frac{1}{n!} S_{1,2}^{(n)} E[(x-x_0)^n] \\
 &= \mathcal{F}(E[x], E[x^2], E[x^3], \dots)
 \end{aligned} \tag{6}$$

127 with $S_{1,2}^{(n)} = \partial S_{1,2}^n(x)/\partial x^n$ computed at an arbitrary point $x = x_0$ and a function $\mathcal{F}_{1,2} \in \mathbb{R}$. Hence the
 128 dynamics of the mean-field $E[V]$ depends on the higher-order statistical orders $E[V^n]$ via the nonlinear
 129 function $E[S_{1,2}(V)]$. This is called the closure problem that is solvable in specific cases only [42].

130 Motivated by previous studies on stochastic bifurcations [43, 44, 45, 46, 47, 48, 49, 50, 51, 52], in which
 131 additive noise may tune the stability close to the bifurcation point, the present work shows how additive
 132 noise strongly impacts the nonlinear dynamics of the system for arbitrary noise intensity and away from
 133 the bifurcation. Previous *ad-hoc* studies have already used mean-field approaches [22, 53, 54] which
 134 circumvents the closure problem (6) through a different mean-field ansatz. These motivational studies left
 135 open a more rigorous derivation. This derivation will be given in the present work: presenting in more
 136 detail its power and its limits of validity.

137 2.3 Equilibria, stability and quasi-cycles

138 The dynamic topology of a model differential equation system may be described partially by the number
 139 and characteristics of its equilibria. In general, for the non-autonomous differential equation system

$$\dot{z} = \mathbf{A}z + \mathbf{N}(z) + \mathbf{I}(t)$$

140 with state variable $z \in \mathbb{R}^N$, the driving force $\mathbf{I} \in \mathbb{R}^N$, the nonlinear vector $\mathbf{N} \in \mathbb{R}^N$ and the matrix
 141 $\mathbf{A} \in \mathbb{R}^{N \times N}$, it is insightful to consider the equilibria of the corresponding autonomous system z_0 with
 142 $\dot{z} = 0$ yielding the implicit condition

$$\mathbf{A}z_0 = -\mathbf{N}(z_0).$$

143 The stability of an equilibrium z_0 is given by the eigenvalue spectrum of the corresponding Jacobian

$$\mathbf{J} = \mathbf{A} + \nabla \mathbf{N}^0$$

144 where $(\nabla \mathbf{N}^0)_{ij} = \partial N_i(z)/\partial z_j$ computed at z_0 . The eigenvalues $\{\lambda_k\}$ of \mathbf{J} can be written as $\lambda_k = a_k +$
 145 $i2\pi\nu_k$ with the damping a_k and the eigenfrequency ν_k . Asymptotically stable equilibria have $\Re(\lambda_k) < 0$,
 146 e.g. stable foci have $a_k < 0$, $\nu_k \in \mathbb{R}$. Linear response theory tells that noise-driven linear systems, whose
 147 deterministic dynamics exhibit a stable focus, exhibit quasi-cycles with a spectral power peak close to
 148 the eigenfrequency, see e.g. [50, 55, 56]. The smaller the noise intensity, the closer is the spectral peak

parameter	description	value
τ_e	exc. synaptic time constant	5ms
τ_i	inhib. synaptic time constant	20ms
F_0	intra-population conn. weight	2.17
M_0	inter-population conn. weight	3.87
c	connection probability	0.95
N	number of network nodes	200
I_e	constant exc. input	1.1
I_i	constant inhib. input	0.4
D_2	inhib. noise variance	0.2
w_{in}	Poisson input weight	2.1
τ_{in}	synaptic time scale of input	5ms
Δt	numerical integration step	0.5ms

Table 1. Parameter set of model (1).

149 frequency to the eigenfrequency. Hence, the eigenfrequency ν_k provides a reasonable estimate of the
 150 quasi-cycle spectral peak.

151 2.4 Numerical simulations

152 The Langevin equations (1) have been integrated over time utilizing the Euler-Maruyama scheme [57].
 153 Table 1 presents the parameters used. In certain cases, the noise variance has been changed over time t
 154 according to

$$D_1(t) = D_{\min} + \frac{D_{\max} - D_{\min}}{T} t \quad (7)$$

155 with the maximum integration time T and the maximum and minimum noise variance values D_{\max} and
 156 D_{\min} , respectively.

158 2.5 Numerical spectral data analysis

159 Since prominent oscillations of the network mean activity indicates synchronised activity in the population,
 160 we have computed the power spectrum of the network mean activity $\bar{V}(t) = \sum_{n=1}^N V_n(t)/N$ employing
 161 the Bartlett-Welch method with overlap rate 0.8. To gain a power spectrum with frequency resolution Δf ,
 162 the Bartlett-Welch segments were chosen to the length $1/\Delta f$ and the time series had a duration of 5s for
 163 the zero-mean Gaussian noise and 8s for the Poisson noise stimulation.

164 In addition to the power spectrum, the synchronisation between single neuron spike activity and the den-
 165 dritic current reflects the degree of coherence in the system. To this end, we have computed the Spike Field
 166 Coherence (SFC) [58]. To estimate the SFC, we have chosen a time window of 5s for zero-mean Gaussian
 167 stimulation and 8s for Poisson stimulation in the Θ - (4Hz-8Hz), α - (8Hz-12Hz), β - (12Hz-20Hz) and
 168 γ - (25Hz-60Hz) frequency band. This standard measure estimates the coherence between spikes $H[V_n](t)$
 169 and their corresponding dendritic currents $V_n(t)$ at the same cell averaged over all cells in the excitatory
 170 population. Significant differences of SFC at different noise intensities are evaluated by an unpaired Welch
 171 t-test with $\alpha = 0.05$.

172

173 2.6 Information measures

174 Coherence quantifies the degree of mutual behavior of different elements. Interestingly, recent studies of
 175 biological neural systems have shown that synchronisation and information content are related [59, 60].
 176 For instance, under general anaesthesia asynchronous cortical activity in conscious patients is accompanied
 177 by less stored information and much available information whereas synchronous cortical activity in
 178 unconscious patients exhibits more stored information and less available information [61, 62, 18, 63, 19].
 179 We are curious how much information is stored and available in coherence resonance described in the
 180 present work. The result may indicate a strong link between coherence and information content. To this end,
 181 we compute the amount of stored information in the excitatory population as the predictable information
 182 and the amount of available information as the population's entropy, cf. [63].

183 The predictable information in the excitatory population is computed as the Active Information Storage
 184 AIS [64, 65] utilizing the Gaussian Copula Mutual Information (GCMI) estimation [66]. Assuming a single
 185 time series $V_i(t)$

$$\text{AIS}_i = \text{MI}(V_i(t); \mathbf{V}_{i\Delta}^{(k)}), \quad \mathbf{V}_{i\Delta}^{(k)} = (V_i(t - \Delta), V_i(t - 2\Delta), \dots, V_i(t - k\Delta)), \quad (8)$$

186 where MI is the mutual information [63, 67], k is the embedding dimension and Δ is the embedding delay.
 187 The value AIS_i describes how much the dendritic current $V_i(t)$ in excitatory neuron i is influenced by its
 188 past. To gain an estimate of stored information in the excitatory population, we evaluate the average stored
 189 information in the population and its variance

$$\begin{aligned} \text{AIS} &= \frac{1}{N} \sum_{i=1}^N \text{AIS}_i \\ \sigma_{\text{AIS}}^2 &= \frac{1}{N-1} \sum_{i=1}^N (\text{AIS}_i - \text{AIS})^2. \end{aligned}$$

190 with $N = 200$. Significant AIS differences at different noise intensities are evaluated by an unpaired Welch
 191 t-test with $\alpha = 0.05$.

192 Moreover, we compute the available information in the excitatory cortex of the dendritic current $V_i(t)$ at
 193 excitatory neuron i as its entropy H_i utilizing the GCMI estimation. Its population average and variance
 194 reads

$$\begin{aligned} H &= \frac{1}{N} \sum_{i=1}^N H_i \\ \sigma_H^2 &= \frac{1}{N} \sum_{i=1}^N (H_i - H)^2. \end{aligned}$$

195 and entropy differences at different noise intensities are evaluated statistically by an unpaired Welch t-test
 196 with $\alpha = 0.05$.

197 In subsequent sections, we have computed AIS and H for embedding dimension $k \in [1; 60]$ and
198 $\Delta \in \{\Delta t, 2\Delta t, 5\Delta t\}$ with $k\Delta = 60$ and find consistent significance test results. Specifically, we have
199 chosen $\Delta = \Delta t$ and $k = 1$ in the shown results.

3 RESULTS

200 The subsequent section shows the derivation of the mean-field equations, before they are applied to describe
201 network dynamics for two types of partial stimulation.

202 3.1 Mean-field description

203 To derive the final equations, we first introduce the idea of a mode projection before deriving the
204 mean-field equations as a projection on the principal mode. The extension to partial stimuli extends the
205 description.

206 Mode decomposition

207 In the model (1), the system activity $\mathbf{V} \in \mathcal{U}$ in space \mathcal{U} may be expanded into a mode basis $\{\Phi_n^e\}$, $n =$
208 $1, \dots, N$, $\Phi_n^e \in \mathbb{C}^N$,

$$\mathbf{V} = \sum_{n=1}^N a_n \Phi_n^e$$

209 with complex mode amplitude $a_n \in \mathbb{C}$ and a biorthogonal basis $\{\Psi_n^e\}$, $\Psi_n^e \in \mathbb{C}^N$ and

$$\Psi_k^{e\dagger} \Phi_n^e = \delta_{kn}, \quad k, n = 1, \dots, N.$$

210 Here, \dagger denotes the transpose complex conjugate. The same holds for \mathbf{W} with the basis $\{\Phi_n^i\}$, $n =$
211 $1, \dots, N$, $\Phi_n^i \in \mathbb{C}^N$,

$$\mathbf{W} = \sum_{n=1}^N b_n \Phi_n^i$$

212 with the complex mode amplitude $b_n \in \mathbb{C}$ and the biorthogonal basis $\{\Psi_n^i\}$, $\Psi_n^i \in \mathbb{C}^N$ and

$$\Psi_k^{i\dagger} \Phi_n^i = \delta_{kn}, \quad k, n = 1, \dots, N.$$

213 Projecting \mathbf{V} , \mathbf{W} onto the respective basis $\{\Psi_k^e\}$ and $\{\Psi_k^i\}$, we obtain amplitude equations

$$\begin{aligned} \tau_e \frac{da_k}{dt} &= -a_k + \Psi_k^{e\dagger} \mathbf{F} \mathbf{S}_1[\mathbf{V}] - \Psi_k^{e\dagger} \mathbf{M} \mathbf{S}_2[\mathbf{W}] \\ &\quad + I^e + \Psi_k^{e\dagger} \boldsymbol{\xi}^e(t) \\ \tau_i \frac{db_k}{dt} &= -b_k + \Psi_k^{i\dagger} \mathbf{M} \mathbf{S}_1[\mathbf{V}] - \Psi_k^{i\dagger} \mathbf{F} \mathbf{S}_2[\mathbf{W}] \\ &\quad + I^i + \Psi_k^{i\dagger} \boldsymbol{\xi}^i(t). \end{aligned}$$

214 Now let us assume that Ψ_k^e, Φ_k^e are eigenvectors of \mathbf{F} with eigenvalue $\lambda_k^e \in \mathbb{C}$

$$\begin{aligned} \mathbf{F} \Phi_k^e &= \lambda_k^e \Phi_k^e \\ \Psi_k^{e\dagger} \mathbf{F} &= \lambda_k^e \Psi_k^{e\dagger} \end{aligned}$$

215 and Ψ_k^i, Φ_k^i are eigenvectors of M with eigenvalue $\lambda_k^i \in \mathbb{C}$

$$\begin{aligned} M\Phi_k^i &= \lambda_k^i \Phi_k^i \\ \Psi_k^{i\dagger} M &= \lambda_k^i \Psi_k^{i\dagger}. \end{aligned}$$

216 Then

$$\begin{aligned} \lambda_1^e &= F_0, \quad \Phi_1^e = e, \quad \Psi_1^e = e/N \\ \lambda_n^e &\approx 0, \quad n = 2, \dots, N, \end{aligned} \tag{9}$$

217 cf. section 2.1, where we have utilized the bi-orthogonality of the basis. Equivalently,

$$\begin{aligned} \lambda_1^i &= M_0, \quad \Phi_1^i = e, \quad \Psi_1^i = e/N \\ \lambda_n^i &\approx 0, \quad n = 2, \dots, N. \end{aligned}$$

218 We observe that $\Psi_1^{i\dagger} = \Psi_1^{e\dagger}$ and $\Phi_1^e = \Phi_1^i$.

219 The vector space \mathcal{U} can be decomposed into complement subspaces $\mathcal{Z}, \mathcal{Z}_\perp$ with $\mathcal{U} = \mathcal{Z} \oplus \mathcal{Z}_\perp$ and
 220 $\Psi_1^e, \Psi_1^i \in \mathcal{Z}$. Then $\Psi_{k>1}^e, \Psi_{k>1}^i \in \mathcal{Z}_\perp$. Each vector $\Psi_{k>1}^i$ can be described in the basis $\Psi_{k>1}^e$ in \mathcal{Z}_\perp and
 221 one gains

$$\begin{aligned} \Psi_{k>1}^{i\dagger} F &= \sum_{n=2}^N c_n \Psi_n^{e\dagger} F \\ &= \sum_{n=2}^N c_n \lambda_n^e \Psi_n^{e\dagger} \\ &= 0 \end{aligned}$$

222 due to (9) and equivalently

$$\begin{aligned} \Psi_{k>1}^{e\dagger} M &= \sum_{n=2}^N c_n \Psi_n^{i\dagger} M \\ &= \sum_{n=2}^N c_n \lambda_n^i \Psi_n^{i\dagger} \\ &= 0 \end{aligned}$$

223 with some coefficients $c_n \in \mathbb{C}$. This yields

$$\begin{aligned} \tau_e \frac{da_1}{dt} &= -a_1 + \frac{\lambda_1^e}{N} e^t \mathbf{S}_1[\mathbf{V}] - \frac{\lambda_1^i}{N} e^t \mathbf{S}_2[\mathbf{W}] \\ &\quad + I^e + m_e(t) \end{aligned} \quad (10)$$

$$\begin{aligned} \tau_i \frac{db_1}{dt} &= -b_1 + \frac{\lambda_1^i}{N} e^t \mathbf{S}_1[\mathbf{V}] - \frac{\lambda_1^e}{N} e^t \mathbf{S}_2[\mathbf{W}] \\ &\quad + I^i + m_i(t) \end{aligned} \quad (11)$$

$$\tau_e \frac{da_k}{dt} = -a_k + \Psi_k^{e\dagger} \xi^e(t), \quad k = 2, \dots, N \quad (12)$$

$$\tau_i \frac{db_k}{dt} = -b_k + \Psi_k^{i\dagger} \xi^i(t), \quad k = 2, \dots, N \quad (13)$$

224 with $m_{e,i}(t) = e^t \xi^{e,i}(t)/N$.

225 The mean-field equations

226 Equations (12), (13) describe an Ornstein-Uhlenbeck process with solution

$$\begin{aligned} a_k(t) &= \int_{-\infty}^t e^{-(t-\tau)/\tau_e} \Psi_k^{e\dagger} \xi^e(\tau) d\tau \\ b_k(t) &= \int_{-\infty}^t e^{-(t-\tau)/\tau_i} \Psi_k^{i\dagger} \xi^i(\tau) d\tau \end{aligned} \quad (14)$$

227 for $t \rightarrow \infty$. In Eqs. (10), (11) the terms \mathbf{V} , \mathbf{W} can be written as

$$\begin{aligned} \mathbf{V} &= \sum_{n=1}^N a_n(t) \Phi_n^e = a_1 \Phi_1^e + \sum_{n=2}^N a_n(t) \Phi_n^e \\ \mathbf{W} &= \sum_{n=1}^N b_n(t) \Phi_n^i = b_1 \Phi_1^i + \sum_{n=2}^N b_n(t) \Phi_n^i. \end{aligned} \quad (15)$$

228 Inserting expressions in Eqs. (14) into these expressions leads to

$$\begin{aligned} \sum_{n=2}^N a_n(t) \Phi_n^e &= \int_{-\infty}^t e^{-(t-\tau)/\tau_e} \sum_{n=2}^N \Phi_n^e \Psi_n^{e\dagger} \xi(\tau) d\tau. \\ \sum_{n=2}^N b_n(t) \Phi_n^i &= \int_{-\infty}^t e^{-(t-\tau)/\tau_i} \sum_{n=2}^N \Phi_n^i \Psi_n^{i\dagger} \xi(\tau) d\tau. \end{aligned} \quad (16)$$

229 By virtue of the completeness of the basis, it is

$$\begin{aligned} \sum_{n=2}^N \Phi_n^e \Psi_n^{e\dagger} &= \mathbf{I} - \Phi_1^e \Psi_1^{e\dagger} \\ \sum_{n=2}^N \Phi_n^i \Psi_n^{i\dagger} &= \mathbf{I} - \Phi_1^i \Psi_1^{i\dagger} \end{aligned}$$

230 with the unity matrix $\mathbf{I} \in \mathbb{R}^{N \times N}$. Then inserting these identities into (16)

$$\begin{aligned} \sum_{n=2}^N a_n(t) \Phi_n^e &= \int_{-\infty}^t e^{-(t-\tau)/\tau_e} \xi^e(\tau) d\tau \\ &\quad - \int_{-\infty}^t e^{-(t-\tau)/\tau_e} \Phi_1^e m_e(\tau) d\tau \\ \sum_{n=2}^N b_n(t) \Phi_n^i &= \int_{-\infty}^t e^{-(t-\tau)/\tau_i} \xi^i(\tau) d\tau \\ &\quad - \int_{-\infty}^t e^{-(t-\tau)/\tau_i} \Phi_1^i m_i(\tau) d\tau. \end{aligned} \tag{17}$$

231 We define $\eta^{e,i}(t) = \xi^{e,i}(t) - \xi_0^{e,i}$, $e^t \eta^{e,i}(t) = N \rho^{e,i}(t)$ with $\rho^{e,i} \sim \mathcal{N}(0, D_{1,2}/N)$ and temporally
 232 constants $\xi_0^{e,i}$, i.e. $\rho^{e,i}$ are finite size fluctuations with variance $D_{1,2}/N$ and $\rho^{e,i} \rightarrow 0$ for $N \rightarrow \infty$. With
 233 the definitions

$$\mathbf{w}_{e,i}(t) = \int_{-\infty}^t e^{-(t-\tau)/\tau_{e,i}} \eta^{e,i}(\tau) d\tau \tag{18}$$

$$\begin{aligned} \mathbf{s}_{e,i}(t) &= \tau_e (\xi_0^{e,i} - e \bar{\xi}_0^{e,i}) \\ &\quad - e \int_{-\infty}^t e^{-(t-\tau)/\tau_{e,i}} \rho^{e,i}(\tau) d\tau \end{aligned} \tag{19}$$

234 with $\bar{\xi}_0^{e,i} = \sum_{n=1}^N \xi_{0,n}^{e,i}/N$ and inserting Eq. (17) into Eqs. (15)

$$\begin{aligned} \mathbf{V}(t) &= a_1(t) \mathbf{e} + \mathbf{s}_e(t) + \mathbf{w}_e(t) \\ \mathbf{W}(t) &= b_1(t) \mathbf{e} + \mathbf{s}_i(t) + \mathbf{w}_i(t) \end{aligned} \tag{20}$$

235 and the mean-field equations can be written as

$$\begin{aligned} \tau_e \frac{da_1}{dt} &= -a_1 + \frac{F_0}{N} e^t \mathbf{S}_1 [a_1(t) \mathbf{e} + \mathbf{s}_e(t) + \mathbf{w}_e(t)] \\ &\quad - \frac{M_0}{N} e^t \mathbf{S}_2 [b_1(t) \mathbf{e} + \mathbf{s}_i(t) + \mathbf{w}_i(t)] \\ &\quad + I^e + \bar{\xi}_0^e + \rho^e(t) \\ \tau_i \frac{db_1}{dt} &= -b_1 + \frac{M_0}{N} e^t \mathbf{S}_1 [a_1(t) \mathbf{e} + \mathbf{s}_e(t) + \mathbf{w}_e(t)] \\ &\quad - \frac{F_0}{N} e^t \mathbf{S}_2 [b_1(t) \mathbf{e} + \mathbf{s}_i(t) + \mathbf{w}_i(t)] \\ &\quad + I^i + \bar{\xi}_0^i + \rho^i(t) \end{aligned} \tag{21}$$

236 By virtue of the finite-size fluctuations over time $\rho^{e,i}(t)$ the system's mean-field obeys stochastic dynamics.

237 Equations (14) describe an Ornstein-Uhlenbeck process of mode k and thus $\mathbf{w}_{e,i}(t)$ describes a multivari-
 238 ate Ornstein-Uhlenbeck process over time. In addition, $\mathbf{w}_{e,i}(t)$ is stationary over time and, since all modes
 239 k share identical properties, it is stationary over the network. Consequently, the process is ergodic and the
 240 stationary probability density function $p(\mathbf{w}_{e,i})$ of $\mathbf{w}_{e,i}$ can be computed over the network yielding

$$\begin{aligned} \frac{1}{N} \mathbf{e}^t \mathbf{S}_1 [x \mathbf{e} + \mathbf{w}] &= \frac{1}{N} \sum_{n=1}^N S[x + w_n] \\ &\approx \int_{-\infty}^{\infty} S(x + w) p_e(w) dw \\ &= G_1(x), \end{aligned} \quad (22)$$

241 where the approximation is good for large N . Specifically, for Gaussian zero-mean uncorrelated noise ξ_e
 242 with variance D [68]

$$p_e(w) = \frac{1}{\sqrt{2\pi}\sigma} e^{-w^2/2\sigma^2}, \quad \sigma^2 = D/\tau_e.$$

243 Similarly,

$$\begin{aligned} \frac{1}{N} \mathbf{e}^t \mathbf{S}_2 [x \mathbf{e} + \mathbf{w}] &\approx \int_{-\infty}^{\infty} S(x + w) p_i(w) dw \\ &= G_2(x) \end{aligned} \quad (23)$$

244 Moreover, if the mean input is $\xi_0^{e,i} = \alpha^{e,i} \mathbf{e}$ and $N \rightarrow \infty$, then $\mathbf{s}_{e,i} = 0$ and $\rho^{e,i} = 0$ and consequently
 245 the mean-field equation

$$\begin{aligned} \tau_e \frac{da_1}{dt} &= -a_1 + F_0 G_1(a_1) - M_0 G_2(b_1) + I^e + \alpha^e \\ \tau_i \frac{db_1}{dt} &= -b_1 + M_0 G_1(a_1) - F_0 G_2(b_1) + I^i + \alpha^i \end{aligned} \quad (24)$$

246 obeys deterministic dynamics. However, the above formulation depends implicitly on the additive noise
 247 through the convolution of the transfer function.

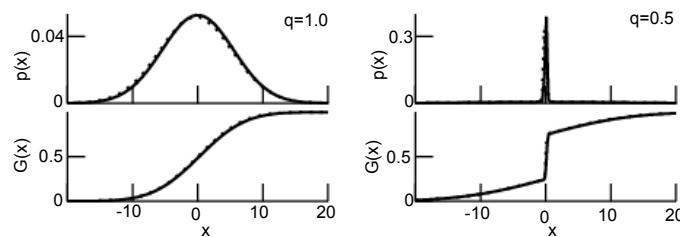


Figure 2. The probability density function p (26) and the resulting transfer function G (27). For $q = 1.0$ $D_1/\tau_e = 0.15$ and for $q = 0.5$ $D_1/\tau_e = 0.5$.

248 Partial stimuli

249 Each noise baseline stimulus at inhibitory neurons $(\xi^i)_n = \xi_n^i$ at network node n is Gaussian distributed
 250 with zero mean and variance D_2 (cf. section 2.1). Then $\bar{\xi}_0^i = 0$, $s_i(t) = \bar{\rho}^i(t) \sim \mathcal{N}(0, D_2/\tau_i N)$ and,
 251 considering Eq. (18), the corresponding probability density function in Eq. (23) is $p_i(w) = \mathcal{N}(0, D_2/\tau_i)$.
 252 Here $\mathcal{N}(0, \sigma^2)$ denotes a normal distribution with zero mean and variance σ^2 .

253 Additionally, stochastic stimuli driving excitatory neurons in class \mathcal{G}_1 are ergodic (cf. section 2.1). Then
 254 the mean and variance of class \mathcal{G}_1 is

$$\begin{aligned} \bar{\xi}_1^e &= \frac{1}{N_1} \sum_{n \in \mathcal{G}_1} \xi_n^e \\ D_1 &= \frac{1}{N_1} \sum_{n \in \mathcal{G}_1} (\xi_n^e)^2. \end{aligned} \tag{25}$$

255 Using Eq. (18) and Eq. (19) and assuming $N \rightarrow \infty$, then

$$w^e(t) + s^e(t) = \int_{-\infty}^t e^{-(t-\tau)/\tau_e} (\eta^e(\tau) + \Delta \xi) d\tau$$

256 whose probability density function $p_e(w)$ is [22]

$$\begin{aligned} p_e(w) &= \sum_{m=1}^2 q_m \mathcal{N}(\bar{\xi}_m^e, D_1^m/\tau_e) \\ &= q \mathcal{N}(\bar{\xi}_1^e, D_1/\tau_e)[w] + (1 - q)\delta(w) \end{aligned} \tag{26}$$

257 with $q = N_1/N$, $q_1 = q$, $q_2 = 1 - q$. Here, $\Delta \xi = (1 - q, 1 - q, \dots, -q, -q)\xi_1^e$ with terms $1 - q$ of number
 258 N_1 and assuming that the nodes $n = 1, \dots, N_1$ receive stochastic input. In addition the constant input in
 259 the mean-field equation is $\bar{\xi}_0^e = q\xi_1^e$.

260 Then, utilizing Eqs. (22), (23) and specifying S to a step function (cf. section 2.1), the mean-field transfer
 261 functions in Eq. (24) read

$$\begin{aligned} G_1(a_1) &= \frac{q}{2} \left[1 - \operatorname{erf} \left(-\frac{a_1 - \xi_1^e}{\sqrt{2D_1/\tau_e}} \right) \right] \\ &\quad + (1 - q)\Theta(a_1) \\ G_2(b_1) &= \frac{1}{2} \left[1 - \operatorname{erf} \left(-\frac{b_1}{\sqrt{2D_2/\tau_i}} \right) \right]. \end{aligned} \tag{27}$$

262 Here, $\Theta(\cdot)$ denotes the Heaviside step function. Figure 2 shows examples for p_e and G_1 .

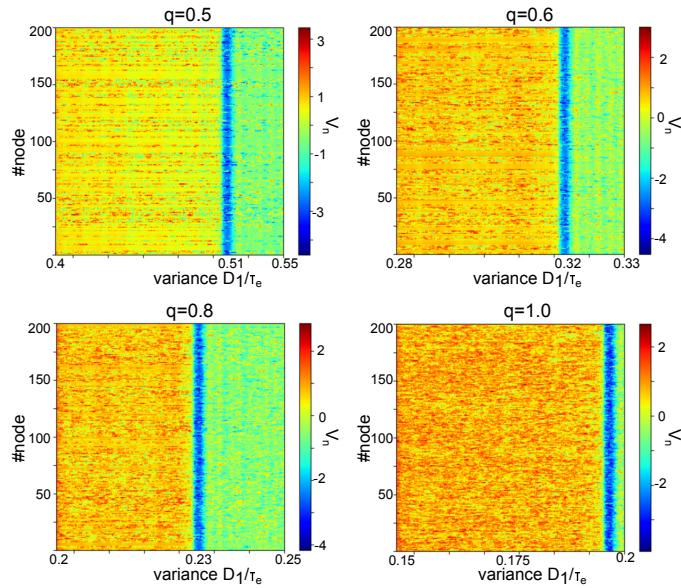


Figure 3. Enhanced zero-mean Gaussian noise induces phase transitions in spatiotemporal dynamics. The panels show the network activity $\mathbf{V}(t)$ according to Eqs. (1) with temporally increasing noise variances D_1/τ_e for different stimulus ratios q .

263 Essentially, the mean-field obeys

$$\begin{aligned}
 \tau_e \frac{da_1}{dt} &= -a_1 + F_0 G_1(a_1) - M_0 G_2(b_1) + I^e \\
 &\quad + \rho^e(t) \\
 \tau_i \frac{db_1}{dt} &= -b_1 + M_0 G_1(a_1) - F_0 G_2(b_1) + I^i \\
 &\quad + \rho^i(t)
 \end{aligned}
 \tag{28}$$

264 utilizing (27).

265 3.2 Zero-mean Gaussian partial stimulation

266 At first, we consider the case of a partial noise stimulation with zero network mean, i.e. $e^t \bar{\xi}^e = 0$ and
 267 $s_e(t) \sim \mathcal{N}(0, D_1/\tau_e N_1)$ and $\xi_1^e = \bar{\xi}_0^e = 0$. Then D_1 parametrizes the noise intensity only. Figure 3 shows
 268 the network evolution of $\mathbf{V}(t)$ for increasing noise intensities, cf. Eqs. (7). Starting from a high activity
 269 state, increasing the noise intensity yields a phase transition of the system to a network state at lower
 270 activity. This occurs for global ($q = 1.0$) and partial stimulation ($q = 0.8, q = 0.6$ and $q = 0.5$). Please
 271 re-call that, for instance, $q = 0.5$ reflects a stimulation where 50% of the network nodes are stimulated.
 272 These stimulated network nodes have been randomly chosen from a uniform distribution.

273 Fig. 4 shows the respective power spectra of the network mean $\mathbf{V}(t)$, which provides insights about the
 274 system's synchronisation at low and high noise intensity. High noise intensity induces strong oscillations
 275 in the γ -frequency band, whereas the low noise intensity states does not - in contrast, this state shows a
 276 decaying low-pass power spectral density that is expected from a non-oscillatory stochastic process.

277 Stronger power spectral density at a given frequency is the signature of a coherent network, as seen in
 278 Fig. 4. Since the neurons in our network model emit spikes and exhibit synaptic input currents, noise-
 279 induced coherence may be visible in the coherence between spiking and synaptic activity as well. In fact,
 280 in Fig. 5(A) one observes a significant strongly enhanced spike-field coherence at high noise intensities for
 281 both global and partial stimulation. Hence, in sum the system exhibits coherence resonance in the sense
 282 that strong noise induces coherent oscillations that are not present at low noise intensities.

283 Coherence resonance is supposed to be linked to information processing in neural systems. Thus
 284 we investigate the relationship between stimulus noise intensity and information in the system across
 285 frequency bands. Figure 5(B) shows how much information is stored in the networks (AIS) and how
 286 much information is available (H). We observe that significantly more information is stored (AIS) and
 287 available (H) at high noise intensities for global stimulation $q = 1.0$, whereas high noise partial stimulation
 288 with $q = 0.8$ diminishes the stored active information and available information significantly. For more
 289 sparse stimulation with $q = 0.6$ the finding in information measures is heterogeneous and no interpretation
 290 consistent with the results for larger q is possible.

291 To understand this noise-induced coherence, we take a closer look at the dynamic topology of the mean-
 292 field equations (28). Their equilibria (cf. section 2.3) for negligible finite-size fluctuations $\rho^{e,i}(t) \ll 1$
 293 are shown in Fig. 6 together with simulated mean-field activity $\bar{V}(t)$ for illustrative purposes. Low noise
 294 intensity induces a bistable regime with a stable node as upper equilibrium and a focus as lower equilibrium.
 295 For global stimulation ($q = 1.0$), this lower focus is unstable at very low noise intensity and stable at
 296 larger noise intensities. Moreover, the lower equilibrium is a stable focus at all noise intensities for partial
 297 ($q < 1.0$) stimulation. The center branch is always a saddle node. For larger noise intensity, the upper
 298 equilibrium branch merges with the center branch via a saddle-node bifurcation and the lower stable focus
 299 is preserved as noise is further increased. This finding remains valid for both global ($q = 1.0$) and partial
 300 ($q < 1.0$) stimulation as shown in Fig. 6 for q ranging within the interval $0.5 \leq q \leq 1.0$. One can see
 301 that for smaller q (i.e. less excitatory neurons are stimulated) the bifurcation point moves to larger noise
 302 intensities. Hence thinning out the stimulation of excitatory neurons increases the noise intensity interval at
 303 which bistability occurs.

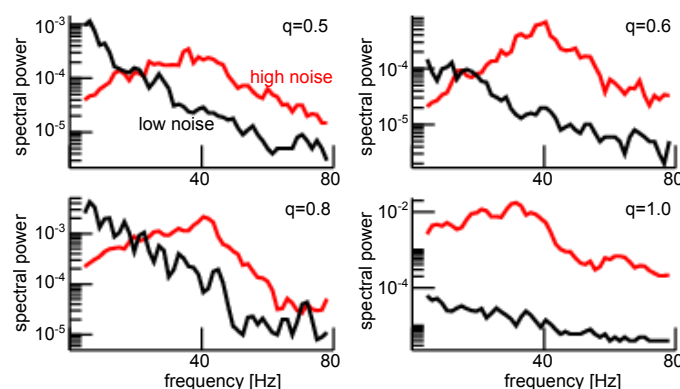


Figure 4. Enhanced noise yields strong power of the global mode $\bar{V}(t)$ in the γ -frequency range. The panels show the power spectra of \bar{V} for the stimulus ratios $q = 0.5$ ($D_1/\tau_e = 0.35$ (black) and $D_1/\tau_e = 0.55$ (red)), $q = 0.6$ ($D_1/\tau_e = 0.25$ (black) and $D_1/\tau_e = 0.33$ (red)), $q = 0.8$ ($D_1/\tau_e = 0.20$ (black) and $D_1/\tau_e = 0.25$ (red)) and $q = 1.0$ ($D_1/\tau_e = 0.15$ (black) and $D_1/\tau_e = 0.20$ (red)). Power spectra at lower noise intensities are computed on the respective upper branch of the bistable system.

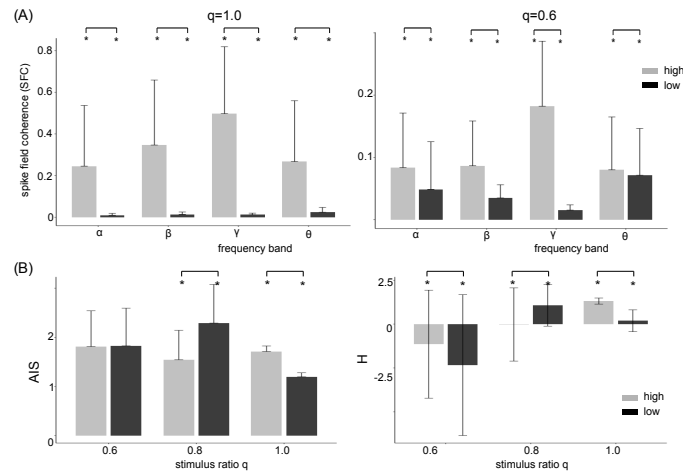


Figure 5. High zero-mean Gaussian noise enhances the Spike-Field Coherence in all frequency bands and affects heterogeneously Active Information Storage (AIS) and differential entropy (H). (A) The differences between high noise intensity (grey-colored) and low noise intensity (black-colored) is significant ($p < 0.001$) for both global and partial stimulation. (B) For global stimulation ($q = 1.0$), high noise intensity induces states of significantly enhanced stored active information (AIS) and available information (H), whereas partial stimulation with $q = 0.8$ diminishes both AIS and H significantly. Results for $q = 0.6$ are not consistent and difficult to interpret. In all panels, vertical bars denote the standard deviation, $p < 0.001$ and parameters are identical to the parameters used in Fig. 4.

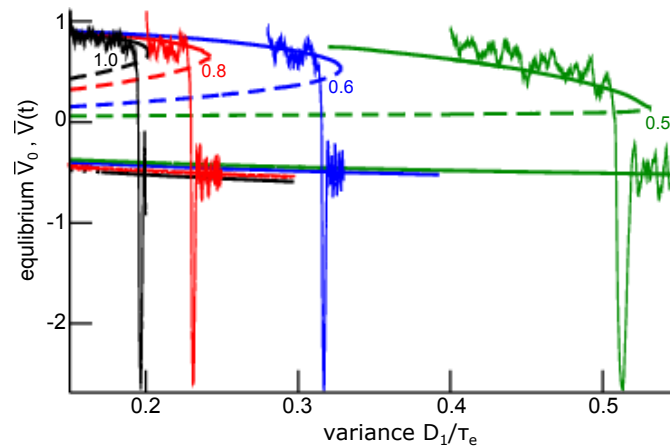


Figure 6. Equilibria and representative time series of the global mode $\bar{V}(t)$ for the zero-mean partial stimulation. There is a bistability and saddle-node bifurcation from a stable node to an stable focus at enhanced noise intensity. The numbers denote the values of the stimulus ratio q . Solid (dashed) lines mark stable (unstable) states. The time series \bar{V} results from the time-varying noise intensity according to Eq. (7.)

304 The frequency range of oscillations observed for steady states located within the lower branch (see Fig.
 305 6) is a consequence of both network connectivity and neuronal properties - and is further tuned by additive
 306 noise. Figure 7 shows the maximum eigenvalue real part for the upper (A) and the lower branch (B, top
 307 opanel) and the eigenfrequency (cf. subsection (2.3)) of the equilibrium at the lower branch (B, lower
 308 panel). We observe that increasing noise intensity decreases slightly the eigenfrequency in the γ -frequency
 309 range and decreases the negative maximum eigenvalue real part. This means that additive noise increases
 310 the damping of the response of the system to perturbations - including noise. This increased noise-induced
 311 damping leads to magnitude changes in quasi-cycle solutions - which is manifested in the power spectral

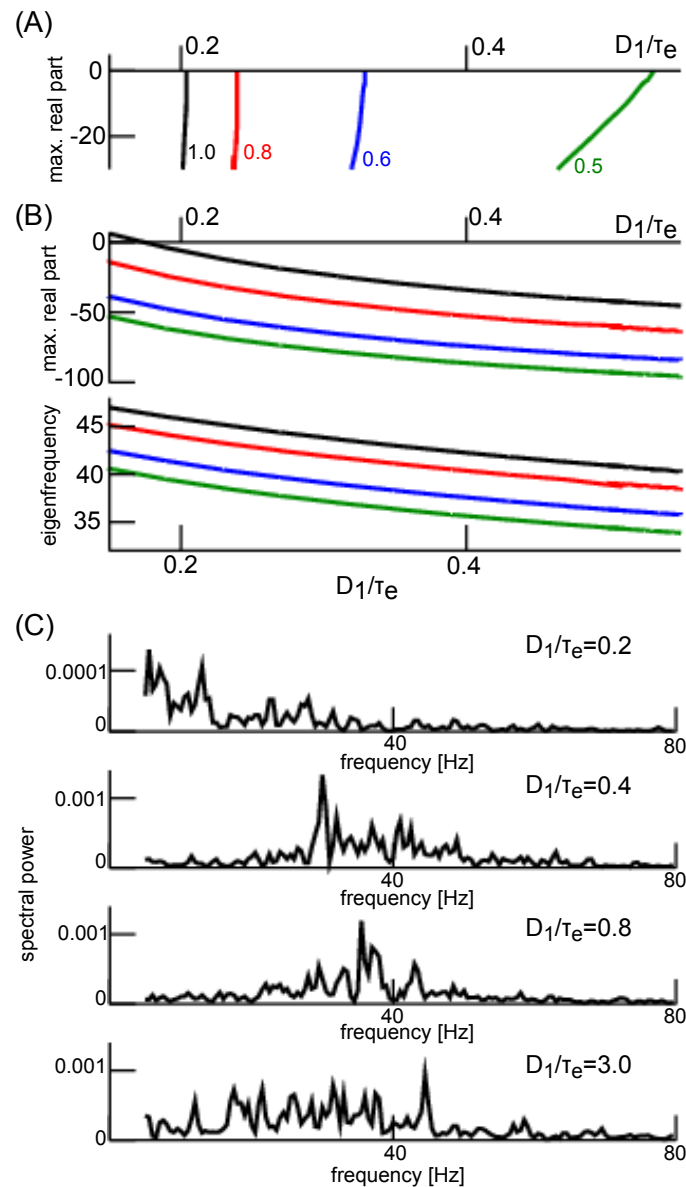


Figure 7. Eigenvalues at the top and bottom branch in Fig. 6 and corresponding power spectra. (A) maximum eigenvalue of equilibria on the top branch in Fig. 6. (B) maximum real part r of the eigenvalue $r + i2\pi\nu$ (top panel) and the corresponding eigenfrequency ν . The numbers denote the values of the stimulus ratio q in all panels. (C) Power spectra of $V(t)$ about the lower branch for $q = 0.6$ for different noise intensities D_1/τ_e .

312 density distribution. Indeed, the power spectral density distribution widens as noise intensity increases,
 313 leading to the spectra as seen in Fig. 7(C). This broad spectral power distribution is the signature of
 314 suppressed coherence. As a corollary, our analysis demonstrates that coherent band-limited oscillations
 315 emerge for intermediate noise intensities only. This is a known feature of coherence resonance.

316 3.3 Poisson partial stimulation

317 Synaptic receptors respond to afferent Poisson-distributed input spike trains, whose properties differ
 318 substantially from the Gaussian noise processes we considered so far. To generalize our results to more
 319 physiological stimuli statistics, we considered a partial Poisson noise stimulation with dependent mean and
 320 variance. Specifically, afferent spike trains at spike rate r_{in} induce random responses at excitatory synapses

321 with time constant τ_{in} and synaptic weight w_{in} . Then

$$\begin{aligned} \mathbf{s}^e(t) &= \tau_e \Delta \boldsymbol{\xi} + \bar{\rho}^e(t) \\ \xi_1^e &= w_{in} r_{in} \tau_{in} \\ D_1 &= w_{in} \xi_0 / 2 \\ \bar{\xi}_0^e &= q \xi_1^e \end{aligned}$$

322 and finite-size fluctuations $\bar{\rho}^e(t) \sim \mathcal{N}(0, D_1/N_1)$. Figure 8(A) illustrates the temporal network activity
 323 for a low and high stimuli firing rates r_{in} . Increasing r_{in} induces a transition from a high-activity to a
 324 low activity state for both global and partial stimulation - similarly as in the Gaussian noise case. The
 325 high-activity state is non-oscillatory while the low-activity state is oscillatory, with frequency found in
 326 the γ -frequency range (Fig. 8(B)). In addition, the low-activity state induced by high Poisson input rate
 327 exhibits a strong spike-field coherence in contrast to the high-activity state (Fig. 8(C)). Moreover, high
 328 stimulation noise increases the stored information and the available information for global stimulation with
 329 $q = 1.0$, cf. Fig. 8(D). Information measures for partial stimulation ($q = 0.6$) are heterogeneous and an
 330 interpretation of results for AIS and H is difficult.

331 These results can be understood by taking a closer look at the dynamic topology of the system. Figure 9
 332 reveals that, for global stimulation ($q = 1.0$), the system has two unstable equilibria and one stable
 333 equilibrium at lower noise intensities. The top branch is a stable node, the center branch a saddle node
 334 and the lower branch an unstable focus. There is a very small noise intensity interval at which the top and
 335 bottom branch are both stable. Increasing the Poisson stimuli firing rate leads to a sudden suppression
 336 of high-activity equilibria through a saddle-node bifurcation. Consequently, the transition observed in
 337 Fig. 8(A) is a jump from the stable node on the top bifurcation branch to the stable focus on the bottom
 338 branch similar to the effect shown in Fig. 3. For partial stimulation ($q = 0.6$), the lower branch exhibits
 339 a stable focus for much lower input firing rates. The saddle-node bifurcation is delayed, leading to an
 340 increased noise intensity interval of bistability. Hence, the system exhibits coherence resonance for Poisson
 341 noise as well.

4 DISCUSSION

342 The present study presents a rigorous derivation of mean-field equations for two nonlinearly coupled non-
 343 sparse Erdős-Rényi networks(ERN) that are stimulated by additive noise. This mean field representation is
 344 made possible through spectral separation: the eigenspectrum of ERN networks exhibits a large spectral
 345 gap between the eigenvalue with largest real part and the rest of the spectrum. We show that the projection
 346 of the network dynamics onto the leading eigenmode represents the mean-field. Its dynamics are shaped
 347 by eigenmodes located in the complement subspace spanned by non-leading eigenmodes. In our model,
 348 the subspace dynamics are governed and influenced by additive noise statistics and they obey an Ornstein-
 349 Uhlenbeck process.

350 We extended the mean-field derivation to various types of additive noise, such as global and partial noise
 351 stimuli (i.e. when only a fraction of the excitatory neurons are stimulated) and for both zero-mean Gaussian
 352 and Poisson noise. Collectively, our analysis shows that additive noise induces a phase transition from a
 353 non-oscillatory state to an oscillatory coherent state. Such noise-induced coherence is known as coherence
 354 resonance (CR). This phase transition has been shown to occur not only for Gaussian zero-mean noise but
 355 also for Poisson noise. To the best of our knowledge, CR has not been found yet for such Poisson noise.

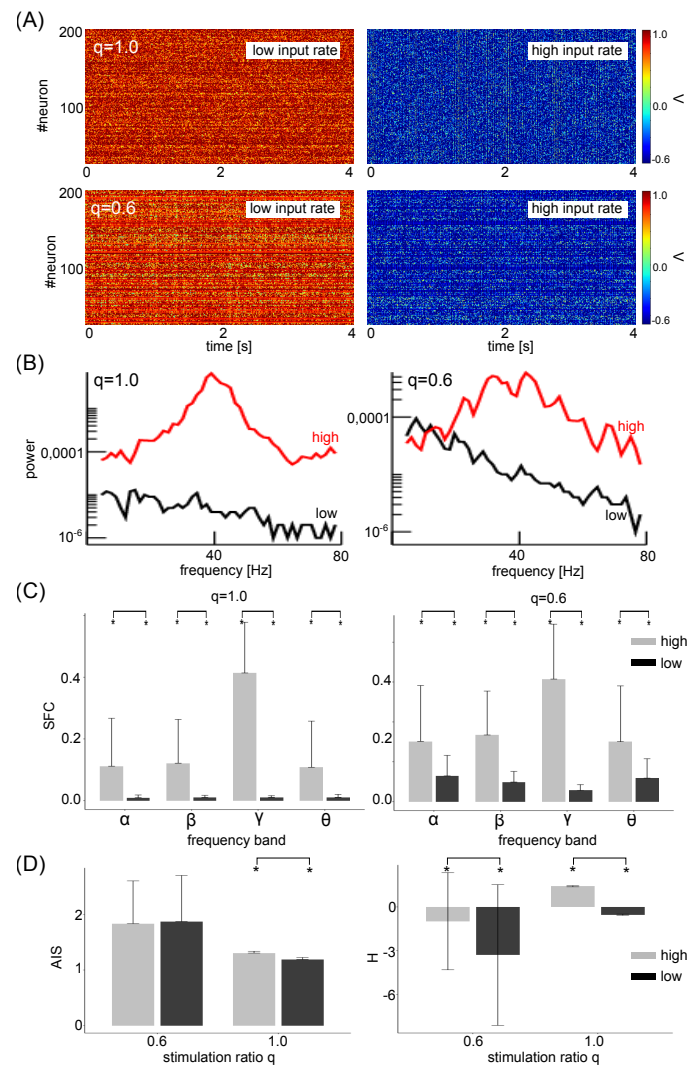


Figure 8. Poisson noise induces transitions from a non-oscillatory to an oscillatory state for both global and partial stimulation. (A) Network activity $V_n(t)$ for low input firing rate ($r = 0.04$ for $q = 1.0$ and $r = 0.09$ for $q = 0.6$) and high input firing rate ($r = 0.14$ for $q = 1.0$ and $r = 0.19$ for $q = 0.6$). For the low (high) input rate the system evolves about an upper (lower) state. (B) Power spectra of the network mean $\bar{V}(t)$ showing γ -activity for the large input rate. (C) The high input firing rate (grey-colored) induces a state of large spike-field coherence compared to the state for low input firing rate (black-colored) for both global and partial stimulation ($p < 0.01$). (D) For global stimulation ($q = 1.0$), high input firing induces a state of significantly enhanced stored active information (AIS) and available information (H). This is not consistent to results for partial stimulation ($q = 0.6$). Here is $p < 0.01$.

356 The general underlying mechanism is a noise-induced multiplicative impact of additive stimulation via
 357 the nonlinear coupling of different modes. This multiplicative effect modifies the net transfer function
 358 of the network and thus enlarges its dynamical repertoire. This resembles the impact of additive noise in
 359 stochastic bifurcations [51, 50, 69, 70]

360 Embedding into literature

361 Our results build on previous studies from the authors [22, 53, 54] to provide a rigorous derivation of the
 362 mean-field description, whereas previous work have motivated heuristically the mean-field reduction and,

363 e.g., failed to show in detail whether the mean-field equation is the only solution for any given additive
364 stimuli. Several other previous studies have presented mean-field descriptions in stochastically driven
365 systems. For instance, Bressloff et al. [27] have derived rigorously mean-field equations for stochastic
366 neural fields considering, inter alia, finite-element fluctuations by utilizing a Master equation and van
367 Kampen's volume expansion approach. We note here that we also took into account finite-size fluctuations
368 resulting from a non-negligible variance of statistical mean values. Moreover, [27] do not specify the
369 network type and results in a rather opaque description, whereas we assume an ERN and thus exploit its
370 unique eigenspectrum structure. This yields directly to a mean-field description, whose dependence of
371 stochastic forces is obvious and avoids its implicit closure problem known from mean-field theories [42].
372 This is possible since the ERN considered share many properties with Ising models, that are known to
373 permit an analytically treatable solution of the closure problem, see e.g. [71].

374 Moreover, several technical analysis steps in the present work have been applied in previous studies in
375 a similar context. In a work on stochastic neural mean-field theory, Faugeras and colleagues [26] have
376 assumed that the system activity fluctuations obey a normal probability distribution and have derived an
377 effective nonlinear interaction in their Proposition 2.1 similar to our Eq. (22). Further, the authors have
378 shown how the fluctuation correlation function, i.e. the system activity's second moment, determine the
379 mean-field dynamics. This is in line with our result (22) showing how the mean and variance of the additive
380 noise tunes the system's stability. However, the authors have not considered in detail the random nature
381 of the system connectivity, whereas we have worked out the interaction of external stimulation and the
382 ERN. This interaction yields directly the mean-field and its dependence of the external stimulus that is
383 not present in [26]. Moreover, the present work also shows how the mean-field fluctuations affect the
384 mean-field dynamics by deriving the fluctuation's probability density function that describes all higher
385 moments.

386 Noise-induced synchronization has been found recently in a system of stochastically-driven linearly
387 coupled FitzHugh-Nagumo neurons by Touboul and colleagues [72]. The authors have found a minimum
388 ratio of activated neurons that are necessary to induce global oscillatory synchronization, i.e. CR in the
389 sense presented in our work. This question has been considered in the present work as well by asking how
390 the mean-field dynamics, and thus how noise-induced synchronization, changes when modifying the ratio
391 of stimulated excitatory neurons q while retaining the stimulation of inhibitory neurons. We find that global
392 stimulation, i.e. stimulation of all excitatory neurons, yields a finite critical noise intensity below which the
393 system is bistable and exhibits CR. Partial stimulation shifts this critical noise intensity to larger values and
394 enlarges the bistability parameter space - and thus promotes CR.

395 Limits and outlook

396 The present work proposes to describe mean-field dynamics in a topological network by projection
397 onto the networks eigenmodes. This works well for non-sparse random ERN with large connectivity
398 probability. This network does not exhibit a spatial structure. However, less connected ERN networks show
399 different dynamics, cf. the Appendix. Moreover, biological networks are not purely random but may exhibit
400 distance-dependent synaptic weights [73] or spatial clusters [74]. Our specific analysis applies for networks
401 with a large spectral gap in their eigenspectra and it might fail for biological networks with smaller spectral
402 gaps (as shown in the Appendix). Future work will attempt to utilize the presented approach to derive
403 mean-field dynamics for heterogeneous networks that exhibit a smaller spectral gap, such as scale-free
404 networks [74].

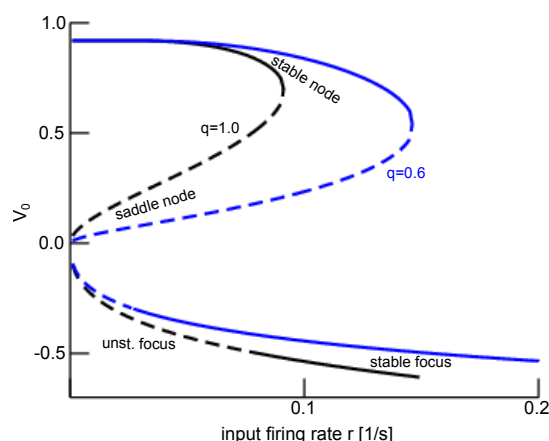


Figure 9. Equilibria of the mean-field $\bar{V}(t)$ for the Poisson partial stimulation. For global stimulation $q = 1.0$, the system is always monostable with three equilibria at low input firing rates and a single equilibrium at large input firing rates. Increasing the input firing rate from low to large firing rates, the system jumps from the upper stationary state (stable node) to a stable focus on the lower stationary state via a saddle-node bifurcation. For partial stimulation $q = 0.6$, the system is monostable with three equilibria at low input firing rates. For larger input rates, the system is bistable and passes a saddle-node bifurcation inducing a transition from a stable node to an stable focus at enhanced input firing rate r . Solid (dashed) lines mark stable (unstable) states, black- and blue-colored lines denote equilibria for global and partial stimulation, respectively. The bifurcation diagram of the mean-field $\bar{W}(t)$ is equivalent.

405 Moreover, the single neuron model in the present work assumes a simple static threshold firing dynamics
 406 (McCullough-Pitts neuron) while neglecting somatic dynamics as described by Hodgkin-Huxley type
 407 models or the widely-used FitzHugh-Nagumo model [10, 72]. Future work will aim at reinforcing the
 408 biological relevance of neurons coupled through ERN.

409 Our results show that noise-induced CR emerges in the γ -frequency range. This frequency band is
 410 thought to play an important role in visual information processing [12, 13, 14, 15, 16]. Experimental
 411 studies have shown that the degree of this γ -synchronization in primary cortical areas may be modulated
 412 by attention [75, 76, 58, 77]. Since attention is known to affect the ARAS activity [78] and specifically the
 413 brain stem as part of the ARAS [79] and ARAS, in turn, provides input to the cortex [80]. We conclude that
 414 it is possible that attention modulates the cortical input activity, i.e. the Poisson firing rate in our model. In
 415 this picture, attention-modulated enhanced ARAS activity induces γ -coherence and may enhance stored
 416 information [81], as shown in Figs. 5 and 8. Future more detailed brain models including the cortico-
 417 thalamic feedback and cortical interactions [56, 20] will provide further evidence whether coherence
 418 resonance is present in visual processing.

REFERENCES

- 419 [1] Pikovsky A, Rosenblum M, Kurths J. *Synchronization: A universal concept in nonlinear sciences*
420 (Cambridge University Press) (2001).
- 421 [2] Singer W. The brain as a self-organising system. *Eur. Arch. Psychiatry Neurol. Sci.* **236** (1986) 4–9.
- 422 [3] Witthaut D, Wimberger S, Burioni R, Timme M. Classical synchronization indicates persistent
423 entanglement in isolated quantum systems. *Nat. Commun.* **8** (2017) 14829.
- 424 [4] Hutt A, Haken H, editors. *Synergetics* (Springer-Verlag, New York) (2020).
- 425 [5] Mompo E, Ruiz-Garcia M, Carretero M, Grahn H, Zhang Y, Bonilla L. Coherence resonance and
426 stochastic resonance in an excitable semiconductor superlattice. *Phys. Rev. Lett.* **121** (2018) 086805.
- 427 [6] Lee C, Choi W, Han JH, Strano M. Coherence resonance in a single-walled carbon nanotube ion
428 channel. *Science* **329** (2010) 1320–1324. doi:10.1126/science.1193383.
- 429 [7] Gu H, Yang M, Li L, Liu Z, Ren W. Experimental observation of the stochastic bursting caused by
430 coherence resonance in a neural pacemaker. *Neuroreport* **13** (2002) 1657–1660.
- 431 [8] Pikovsky A, Kurths J. Coherence resonance in a noise-driven excitable system. *Phys. Rev. Lett.* **78**
432 (1997) 775–778.
- 433 [9] Gang H, Ditzinger T, Ning C, Haken H. Stochastic resonance without external periodic force. *Phys.*
434 *Rev. Lett.* **71** (1993) 807–810.
- 435 [10] Baspinar E, Schüler L, Olmi S, Zakharova A. Coherence resonance in neuronal populations: mean-field
436 versus network model. *submitted* (2020).
- 437 [11] Tönjes R, Fiore C, Pereira T. Coherence resonance in influencer networks. *Nat. Commun.* **12** (2021)
438 72. doi:10.1038/s41467-020-20441-4.
- 439 [12] Singer W, Gray C. Visual feature integration and the temporal correlation hypothesis. *Ann. Rev.*
440 *Neurosc.* **18** (1995) 555–586.
- 441 [13] Eckhorn R, Bauer R, Jordan W, Brosch M, Kruse W, Munk M, et al. Coherent oscillations: a
442 mechanism of feature linking in the visual cortex? multiple electrode and correlation analyses in the
443 cat. *Biol Cybern* **60** (1988) 121–130.
- 444 [14] Castelo-Branco M, Neuenschwander S, Singer W. Synchronization of visual response between the
445 cortex, lateral geniculate nucleus, and retina in the anesthetized cat. *J. Neurosci.* **18** (1998) 6395–6410.
- 446 [15] Nelson J, Salin P, Munk M, Arzi M, Bullier J. Spatial and temporal coherence in cortico-cortical
447 connections: a cross-correlation study in areas 17 and 18 in the cat. *Vis. Neurosci* **9** (1992) 21–37.
- 448 [16] Bressler S. Interareal synchronization in the visual cortex. *Beh. Brain Res.* **76** (1996) 37–49.
- 449 [17] Munk M, Roelfsema P, König P, Engel A, Singer W. Role of reticular activation in the modulation of
450 intracortical synchronization. *Science* **272** (1996) 271–274.
- 451 [18] Hutt A, Lefebvre J, Hight D, Sleigh J. Suppression of underlying neuronal fluctuations mediates EEG
452 slowing during general anaesthesia. *Neuroimage* **179** (2018) 414–428.
- 453 [19] Hutt A. Cortico-thalamic circuit model for bottom-up and top-down mechanisms in general anesthesia
454 involving the reticular activating system. *Arch. Neurosci.* **6** (2019) e95498. doi:10.5812/ans.95498.
- 455 [20] Hutt A, Lefebvre J. Arousal fluctuations govern oscillatory transitions between dominant γ and α
456 occipital activity during eyes open/closed conditions. *submitted* (2021).
- 457 [21] Pisarchik A, Maksimenko V, Andreev A, Frolov N, Makarov V, Zhuravlev M, et al. Coherent
458 resonance in the distributed cortical network during sensory information processing. *Sci. Rep.* **9** (2019)
459 18325. doi:10.1038/s41598-019-54577-1.
- 460 [22] Hutt A, Lefebvre J, Hight D, Kaiser H. Phase coherence induced by additive gaussian and non-gaussian
461 noise in excitable networks with application to burst suppression-like brain signals. *Front. Appl. Math.*

- 462 *Stat.* **5** (2020) 69. doi:10.3389/fams.2019.00069.
- 463 [23] Chacron MJ, Longtin A, Maler L. The effects of spontaneous activity, background noise and the
464 stimulus ensemble on information transfer in neurons. *Network Comput. Neural Syst.* **14** (2003)
465 803–824.
- 466 [24] Chacron MJ, Lindner B, Longtin A. Noise shaping by interval correlations increases information
467 transfer. *Phys.Rev.Lett.* **93** (2004) 059904.
- 468 [25] Chacron MJ, doiron B, Maler L, Longtin A, Bastian J. Non-classical receptive field mediates switch
469 in a sensory neuron's frequency tuning. *Nature* **423** (2003) 77–81. doi:10.1038/nature01590.
- 470 [26] Faugeras OD, Touboul JD, Cessac B. A constructive mean-field analysis of multi population neural
471 networks with random synaptic weights and stochastic inputs. *Front. Comput. Neurosci.* **3** (2008) 1.
- 472 [27] Bressloff PC. Stochastic neural field theory and the system size expansion. *SIAM J. Appl. Math.* **70**
473 (2009) 1488–1521.
- 474 [28] Terney D, Chaieb L, Moliadze V, Antal A, Paulus W. Increasing human brain excitability by
475 Transcranial High-Frequency Random Noise Stimulation. *J. Neurosci.* **28** (2008) 14147–14155.
- 476 [29] Erdős L, Knowles A, Yau H, JYin. Spectral statistics of erdos-renyi graphs i: Local semicircle law.
477 *Ann. Prob.* **41** (2013) 2279–2375. doi:10.1214/11-AOP734.
- 478 [30] Ding X, Jiang T. Spectral distributions of adjacency and laplacian matrices of random graphs. *Ann.*
479 *Appl. Prob.* **20** (2010) 2086–2117.
- 480 [31] Kadavankandy A. *Spectral analysis of random graphs with application to clustering and sampling.*
481 Ph.D. thesis, Université Cote d'Azur (2017). NNT : 2017AZUR4059.
- 482 [32] Füredi Z, Komlos J. The eigenvalues of random symmetric matrices. *Combinatorica* **1** (1981)
483 233–241.
- 484 [33] O'Rourke S, Vu V, Wang K. Eigenvectors of random matrices: A survey. *Journal of Combinatorial*
485 *Theory, Series A* **144** (2016) 361–442. doi:https://doi.org/10.1016/j.jcta.2016.06.008. Fifty Years of
486 the Journal of Combinatorial Theory.
- 487 [34] Koch C. *Biophysics of Computation* (Oxford University Press, Oxford) (1999).
- 488 [35] Ross S. *Stochastic processes (Probability and Mathematical Statistics)* (Wiley) (1982).
- 489 [36] Wright J, Kydd R. The electroencephalogram and cortical neural networks. *Network* **3** (1992)
490 341–362.
- 491 [37] Nunez P. Toward a quantitative description of large-scale neocortical dynamic function and EEG.
492 *Behav. Brain Sci.* **23** (2000) 371–437.
- 493 [38] Nunez P, Srinivasan R. *Electric Fields of the Brain: The Neurophysics of EEG* (Oxford University
494 Press, New York - Oxford) (2006).
- 495 [39] Wilson H, Cowan J. Excitatory and inhibitory interactions in localized populations of model neurons.
496 *Biophys. J.* **12** (1972) 1–24.
- 497 [40] Gerstner W, Kistler W. *Spiking Neuron Models* (Cambridge University Press, Cambridge) (2002).
- 498 [41] Bressloff PC, Coombes S. Physics of the extended neuron. *Int. J. Mod. Phys. B* **11** (1997) 2343–2392.
- 499 [42] Kuehn C. Moment-closure - a brief review. Schöll E, Klapp S, Hövel P, editors, *Control*
500 *of Self-Organizing Nonlinear Systems* (Springer, Heidelberg) (2016), 253–271. doi:10.1007/
501 978-3-319-28028-8_13.
- 502 [43] Sri Namachchivaya N. Stochastic bifurcation. *Applied Mathematics and Computation* **39** (1990)
503 37s–95s. doi:https://doi.org/10.1016/0096-3003(90)90003-L.
- 504 [44] Berglund N, Gentz B. Geometric singular perturbation theory for stochastic differential equations. *J.*
505 *Diff. Eq.* **191** (2003) 1–54.

- 506 [45] Bloemker D, Hairer M, Pavliotis GA. Modulation equations: Stochastic bifurcation in large domains.
507 *Commun. Math. Phys.* **258** (2005) 479–512.
- 508 [46] Boxler P. A stochastic version of the center manifold theorem. *Prob. Th. Rel. Fields* **83** (1989)
509 509–545.
- 510 [47] Hutt A, Lefebvre J. Stochastic center manifold analysis in scalar nonlinear systems involving
511 distributed delays and additive noise. *Markov Proc. Rel. Fields* **22** (2016) 555–572.
- 512 [48] Lefebvre J, Hutt A, LeBlanc V, Longtin A. Reduced dynamics for delayed systems with harmonic or
513 stochastic forcing. *Chaos* **22** (2012) 043121.
- 514 [49] Hutt A. Additive noise may change the stability of nonlinear systems. *Europhys. Lett.* **84** (2008)
515 34003.
- 516 [50] Hutt A, Longtin A, Schimansky-Geier L. Additive noise-induced Turing transitions in spatial systems
517 with application to neural fields and the Swift-Hohenberg equation. *Physica D* **237** (2008) 755–773.
- 518 [51] Hutt A, Longtin A, Schimansky-Geier L. Additive global noise delays Turing bifurcations. *Phys. Rev.*
519 *Lett.* **98** (2007) 230601.
- 520 [52] Hutt A, Lefebvre J. Additive noise tunes the self-organization in complex systems. Hutt A, Haken H,
521 editors, *Synergetics* (Springer, New York), Encyclopedia of Complexity and Systems Science Series
522 (2020), 183.
- 523 [53] Lefebvre J, Hutt A, Knebel J, Whittingstall K, Murray M. Stimulus statistics shape oscillations in
524 nonlinear recurrent neural networks. *J. Neurosci.* **35** (2015) 2895–2903.
- 525 [54] Hutt A, Mierau A, Lefebvre J. Dynamic control of synchronous activity in networks of spiking
526 neurons. *PLoS One* **11** (2016) e0161488. doi:10.1371/journal.pone.0161488.
- 527 [55] Hutt A, Sutherland C, Longtin A. Driving neural oscillations with correlated spatial input and
528 topographic feedback. *Phys.Rev.E* **78** (2008) 021911.
- 529 [56] Hashemi M, Hutt A, Sleigh J. How the cortico-thalamic feedback affects the EEG power spectrum
530 over frontal and occipital regions during propofol-induced anaesthetic sedation. *J. Comput. Neurosci.*
531 **39** (2015) 155.
- 532 [57] Klöden PE, Platen E. *Numerical Solution of Stochastic Differential Equations* (Springer-Verlag,
533 Heidelberg) (1992).
- 534 [58] Fries P, Reynolds J, Rorie A, Desimone R. Modulation of oscillatory neuronal synchronization by
535 selective visual attention. *Science* **291** (2001) 1560–1563.
- 536 [59] Tononi G. An information integration theory of consciousness. *BMC Neurosci.* **5** (2004) 42.
- 537 [60] Alkire M, Hudetz A, G Tononi. Consciousness and anesthesia. *Science* **322** (2008) 876–880. doi:10.
538 1126/science.1149213.
- 539 [61] Lee M, Sanders R, SK Yeom DW, Seo K, Kim H, Tononi G, et al. Network properties in transitions
540 of consciousness during propofol-induced sedation. *Sci. Rep.* **7** (2017) 16791.
- 541 [62] Massimini M, Ferrarelli F, Huber R, Esser SK, Singh H, Tononi G. Breakdown of cortical effective
542 connectivity during sleep. *Science* **309** (2005) 2228–2232.
- 543 [63] Wollstadt P, Sellers K, Rudelt L, Priesemann V, Hutt A, Frohlich F, et al. Breakdown of local
544 information processing may underlie isoflurane anesthesia effects. *PLoS Comput. Biol.* **13** (2017)
545 e1005511.
- 546 [64] Lizier J, Prokopenko M, Zomaya A. Local measures of information storage in complex distributed
547 computation. *Information Science* **208** (2012) 39–54.
- 548 [65] Wibral M, Lizier J, Vögler S, Priesemann V, Galuske R. Local active information storage as a tool to
549 understand distributed neural information processing. *Front. Neuroinform.* **8** (2014) 1.

- 550 [66] Ince R, Giordano B, CKayser, Rousselet G, Gross J, Schyns P. A statistical framework for neuroimag-
551 ing data analysis based on mutual information estimated via a gaussian copula. *Hum. Brain Mapp.* **38**
552 (2017) 1541–1573.
- 553 [67] Wibrals M, Pampu N, Priesemann V, Seiwert FSH, Lindner M, J T Lizier RV. Measuring information-
554 transfer delays. *PLoS One* **8** (2013) 2.
- 555 [68] Risken H. *The Fokker-Planck equation — Methods of solution and applications* (Berlin: Springer)
556 (1989).
- 557 [69] Arnold L. *Random Dynamical Systems* (Springer-Verlag, Berlin) (1998).
- 558 [70] Xu C, Roberts A. On the low-dimensional modelling of Stratonovich stochastic differential equations.
559 *Physica A* **225** (1996) 62–80.
- 560 [71] Derrida B, Gardner E, Zippelius A. An exactly solvable asymmetric neural network model.
561 *Europhys. Lett.* **4** (1987) 187.
- 562 [72] Touboul JD, Piette C, Venance L, Ermentrout G. Noise-induced synchronization and antiresonance in
563 interacting excitable systems: Applications to deep brain stimulation in parkinson’s disease. *Phys. Rev.*
564 *X* **10** (2019) 011073. doi:10.1103/PhysRevX.10.011073.
- 565 [73] Hellwig B. A quantitative analysis of the local connectivity between pyramidal neurons in layers 2/3
566 of the rat visual cortex. *Biol.Cybern.* **82** (2000) 111–121.
- 567 [74] Yan G, Martinez N, Liu YY. Degree heterogeneity and stability of ecological networks. *J. R. Soc.*
568 *Interface* **14** (2017) 20170189. doi:10.1098/rsif.2017.0189.
- 569 [75] Steinmetz P, Roy A, Fitzgerald P, Hsiao S, Johnson K, Niebur E. Attention modulates synchronized
570 neuronal firing in primate somatosensory cortex. *Nature* **404** (2000) 187–190.
- 571 [76] Coull J. Neural correlates of attention and arousal: insights from electrophysiology, functional
572 neuroimaging and psychopharmacology. *Prog. Neurobiol.* **55** (201998) 343–361. doi:10.1016/
573 s0301-0082(98)00011-2.
- 574 [77] Lakatos P, Szilagyi N, Pincze Z, Rajkai C, Ulbert I, Karmos G. Attention and arousal related
575 modulation of spontaneous gamma-activity in the auditory cortex of the cat. *Brain Res. Cogn. Brain*
576 *Res.* **19** (2004) 1–9. doi:10.1016/j.cogbrainres.2003.10.023.
- 577 [78] Kinomura S, Larsson J, Gulyas B, Roland P. Activation by attention of the human reticular formation
578 and thalamic intralaminar nuclei. *Science* **271** (1996) 512–515. doi:10.1126/science.271.5248.512.
- 579 [79] Galbraith G, Olfman D, Huffman T. Selective attention affects human brain stem frequency-following
580 response. *Neuroreport* **14** (2003) 735–738. doi:10.1097/00001756-200304150-00015.
- 581 [80] Koval’zon V. Ascending reticular activating system of the brain. *Transl. Neurosci. Clin.* **2** (2016)
582 275–285. doi:10.18679/CN11-6030/R.2016.034.
- 583 [81] Serences J. Neural mechanisms of information storage in visual short-term memory. *Vision Research*
584 **128** (2016) 53–67. doi:10.1016/j.visres.2016.09.010.